WORLD OCEAN CIRCULATION

PRODUCT USER MANUAL

NAME OF PRODUCTS

(THEME NUMBER)

customer	ESA/ESRIN
ESA contract	ESA Contract No. 4000130730/20/I-NB
document reference	WOC-ESA-ODL-NR-010_PUG_T2_upwelling_indices_V1.0
Version/Rev	1.0
Date of issue	17/07/2021

Issued by	Emmanuelle Autret (Ifremer)
Approved by	Gilles Larnicol (OceanDataLab/Magellium)
Approved by	Marie-Hélène Rio (ESA)

Distribution List

	Name	Organization	Nb. copies
Sent to :	M.H. rio	ESA/ESRIN	ESA-STAR
Internal copy :	Project Manager	OceanDatalab	1 (digital copy)

Document evolution sheet

Ed.	Rev.	Date	Purpose evolution	Comments
1	0	17/07/2021	Creation of document	

Contents

List Of Images

List Of Tables

1 Introduction

1.1 Purpose of the document

The present document is the Product User Manual dedicated to the content and format description of the following products:

- Wind based upwelling flows & transport
- SST-based upwelling indices
- Wond-based & SST-based indices and stations

This is the primary document that users should read before handling the products. It provides an overview of processing algorithms, technical product content and format and main validation results.

1.2 Document structure

In addition to this introduction, this document includes the following chapters:

- Chapter 2 presents the product providing the wind-based upwelling indices (EKT and EKP daily fields)
- Chapter 3 presents the upwelling indices derived from SST data
- Chapter 4 is dedicated to synthetic product including wind-based and SST-based indices at predefined stations

1.3 Applicable & Reference documents

- [RD-1] ESA WOC2019: http://woc2019.esa.int/index.php

- [RD-2] Synthesis of the WOC2019 User Consultation Meeting recommendations http://woc2019.esa.int/files/WOC2019_summary_synthesis.pdf
- [RD-3] Chelton, D., S.-P. Xie (2010), Coupled ocean-atmosphere interactions at oceanic mesoscales, Oceanography, 23, 52–69.
- [RD-4] Bakun, A. (1973), Coastal upwelling indices, west coast of North America, 1946–71, NOAA Tech. Rep. NMFS SSRF-671, 103 pp.
- [RD-5] Bakun, A. (1990), Global climate change and intensification of coastal ocean upwelling, Science, 247, 198–201.
- [RD-6] Chelton, D. (1982), Large-scale response of the California current to forcing by the wind stress curl, CalCOFI Rep., 119, 130–148.

- [RD-7] Halpern, D. (2002).,Offshore Ekman transport and Ekman pumping off Peru during the 1997–1998 El Nino. Geophys. Res. Lett., 29, 1075. doi:10.1029/2001GL014097.
- [RD-8] Pickett, M. H., J. D. Paduan (2003), Ekman transport and pumping in the California Current based on the U.S. Navy's high-resolution atmospheric model (COAMPS), J. Geophys. Res., 108, doi:10.1029/2003JC001902.
- [RD-9] Capet, X.J., P. Marchesiello, J.C. McWilliams (2004), Upwelling response to coastal wind profiles. Geophys. Res. Lett., 31, L13311. Doi:10.1029/ 2004GL020123.
- [RD-10] Castelao, R. M. (2012), Sea surface temperature and wind stress curl variability near a cape. J. Phys. Oceanogr., 42, 2073–2087.
- [RD-11] Marchesiello, P., P. Estrade (2010), Upwelling limitation by onshore geostrophic flow. J. Mar. Res., 68, p. 37-62. ISSN 0022-2402
- [RD-12] Estrade, P., Marchesiello, P., De Verdière, A.C., C. Roy (2008), Cross-shelf structure of coastal upwelling : a two – dimensional extension of Ekman's theory and a mechanism for inner shelf upwelling shut down. J. Mar. Res., 66, http://dx.doi.org/10.1357/002224008787536790
- *[RD-13] - no reference*
- [RD-14] Bentamy, A., D. Croize-Fillon (2012), Gridded surface wind fields from Metop/ASCAT measurements. Inter. Journal of Remote Sensing, 33, 1729-1754. DOI 10.1080/01431161.2011.600348.
- [RD-15] Desbiolles F., Blanke B., Bentamy A., Roy Claude. (2016). Response of the Southern Benguela upwelling system to fine-scale modifications of the coastal wind. J. Mar. Sys., 156, 46-55. ISSN 0924-7963
- [RD-16] Stommel, H. M. (1958), The Gulf Stream: A Physical and Dynamical Description, 202 pp., Univ. Calif. Press, Berkeley, Calif.
- [RD-17] Risien, C.M., D.B. Chelton (2008), A Global Climatology of Surface Wind and Wind Stress Fields from Eight Years of QuikSCAT Scatterometer Data. J. Phys. Oceanogr., 38, 2379-2413.
- [RD-18] Marchesiello, P., P. Estrade (2010), Upwelling limitation by onshore geostrophic flow. J. Mar. Res., 68, p. 37-62. ISSN 0022-2402
- [RD-19] Renault, L., A. Hall, and J. C. McWilliams (2015), Orographic shaping of U.S. West Coast wind profiles during the upwelling season. Climate Dyn., 46, 273–289, doi:https://doi.org/10.1007/s00382-015-2583-4.
- [RD-20] Jacox, M. G., C. A. Edwards, E.L. Hazen, S.J. Bograd (2018) Coastal upwelling revisited, Ekman, Bakun, and improved upwelling indices for the U.S. West Coast. J. Geophys. Res. Oceans, 123, https://doi.org/10.1029/2018JC014187.
- [RD-21] Wang, Y.H., R.K. Walter, C. White, H.K. Farr, B.I. Ruttenberg (2019), Assessment of surface wind datasets for estimating offshore wind energy along the Central California Coast. Renew. Energy, 133, pp. 343-353. https://doi.org/10.1016/j.renene.2018.10.008
- [RD-22] Carvalho, D., A. Rocha, M. Gómez-Gesteira, C. Silva Santos (2014), Comparison of reanalyzed, analyzed, satellite-retrieved and NWP modelled winds with buoy data along the Iberian Peninsula coast. Remote Sens. Environ., 152, 480–492.
- [RD-23] Atlas, R., R.N. Hoffman, J. Ardizzone, S.M. Leidner, J.C. Jusem, D.K. Smith, D. Gombos (2011), A cross-calibrated, multiplatform ocean surface wind velocity product for meteorological and oceanographic applications, B. Amer. Meteorol. Soc., 92, 157–174.

- [RD-24] Hersbach, H., D. Dee (2016), ERA5 reanalysis is in production, ECMWF Newsletter 147, ECMWF, Reading, UK.
- [RD-25] Quilfen Yves, Shutler J., Piolle Jean-Francois, Autret Emmanuelle (2021). Recent trends in the wind-driven California current upwelling system . Remote Sensing of Environment , 261, 112486 (17p.) . https://doi.org/10.1016/j.rse.2021.112486
- [RD-26] Reynolds, R. W., Chelton, D. B., Roberts-Jones, J., Martin, M. J., Menemenlis, D., Merchant, C. J., 2013. Objective determination of feature resolution in two sea surface temperature analyses. Journal of Climate 26 (8), 2514#2533
- [RD-27] Merchant, C. J., Embury, O., Bulgin, C. E., Block, T., Corlett, G. K., Fiedler, E., ... & Eastwood, S. (2019). Satellite-based time-series of sea-surface temperature since 1981 for climate applications. Scientific data, 6(1), 1-18.
- [RD-28] Wooster, W.S., Bakun, A., McLain, D., 1976. The seasonal upwelling cycle along the eastern boundary of the North Atlantic. J. Mar. Res. 34 (2), 131–141.
- [RD-29] Nykjær, L., Van Camp, L., 1994. Seasonal and interannual variability of coastal upwelling along northwest Africa and Portugal from 1981 to 1991. J. Geophys. Res. 99 (C7), 14197–14207.
- [RD-30] Marcello, J., Hernandez-Guerra, A., Eugenio, F., Fonte, A., 2011. Seasonal and temporal study of the northwest African upwelling system. Int. J. Remote Sens. 32, 1843–1859.
- [RD-31] Santos, F., Gomez Gesteira, M., deCastro, M., Alvarez, I., 2011. Differences in coastal and oceanic SST trends due to the strengthening of coastal upwelling along the Benguela Current system. Cont. Shelf Res., 79–86, http://dx.doi.org/10.1016/j.csr.
- [RD-32] Lathurilère, C., Echevin, V., Lévy, M., 2008. Seasonal and intraseasonal surface chlorophyll-a variability along the northwest African coast. J. Geophys. Res. 113, C05007, http://dx.doi.org/10.1029/2007JC004433.
- [RD-33] Nascimento, S., & Franco, P. (2009, October). Unsupervised fuzzy clustering for the segmentation and annotation of upwelling regions in sea surface temperature images. In International Conference on Discovery Science (pp. 212-226). Springer, Berlin, Heidelberg.
- [RD-34] Nascimento, S.; Franco, P. Segmentation of upwelling regions in sea surface temperature images via unsupervised fuzzy clustering. International Conference on Intelligent Data Engineering and Automated Learning. Springer, 2009
- [RD-35] Coelho-Souza, S. A., López, M. S., Guimarães, J. R. D., Coutinho, R., & Candella, R. N. (2012). Biophysical interactions in the Cabo Frio upwelling system, Southeastern Brazil. *Brazilian Journal of Oceanography*, *60*, 353-365.
- [RD-36] Tamim. Segmentation et classification des images satellitaires : application à la détection des zones d'upwelling côtier marocain et mise en place d'un logiciel de suivi spatiotemporel, 2015.
- [RD-37] Nascimento, S., Casca, S., & Mirkin, B. (2015). A seed expanding cluster algorithm for deriving upwelling areas on sea surface temperature images. Computers & Geosciences, 85, 74-85.
- [RD-38] Turi, G., Z. Lachkar, N. Gruber, M. Münnich (2016) Climatic modulation of recent trends in ocean acidification in the California Current System. Envir. Res. Lett. 11, 014007.

1.4 Terminology

ACCUA	Analisi della dinamica della Corrente CircUmpolare Antartica
AMSR2	Advanced Microwave Scanning Radiometer 2
ADT	Absolute Dynamic Topography
AI	Artificial Intelligence
AIL	Action Items List
AIS	Automatic Identification System
ASAR	Advanced Synthetic Aperture Radar
ASCAT	Advanced SCATterometer
ATBD	Algorithm Theoretical Basis Document
AVHRR	Advanced Very High Resolution Radiometer
CCD	Contract Closure Document
CCI	Climate Change Initiative
CCMP	Cross-Calibrated Multi-Platform
CFOSAT	Chinese-French Oceanography Satellite
CIESM	Mediterranean Science Commission
CMEMS	Copernicus Marine Environment Monitoring Service
CNES	Centre National d'Etudes Spatiales
CNR	Consiglio Nazionale delle Ricerche
CTD	Conductivity, Temperature and Depth
DP	Data Pool
DTU	Danmarks Tekniske Universitet
DUACS	Data Unification and Altimeter Combination System
EBUS	Eastern Boundary Upwelling System
ECCO	Estimating the Circulation & Climate of the Ocean
ECMWF	European Centre for Medium-Range Weather Forecasts
EFARO	European Fisheries and Aquaculture Research Organisations
EMB	European Marine Board
ENVISAT	Environmental Satellite
EO	Earth Observation
EPB	European Polar Board
EOEP-5	5th Earth Observation Envelope Programme (2017-2021)
ERA	ECMWF Reanalysis
ESA	European Space Agency
ESF	European Science Foundation
EU	European Union
EuroGOOS	European Global Ocean Observing System
FAO	Food and Agriculture Organization of the United Nations
FR	Final Report

FSLE	Finite Size Lyapunov Exponent
GCM	Global Circulation Model
GOCE	Gravity Field and Steady-State Ocean Circulation Explorer
GOOS	Global Ocean Observing System
GMI	Global precipitation monitoring Microwave Imager
GMM	Gaussian Mixture Models
HYCOM	Hybrid Coordinate Ocean Model
IAR	Impact Assessment Report
ICCAT	International Commission for the Conservation of Atlantic Tunas
ICSU	International Council for Science
IGPB	International Geosphere-Biosphere Programme
IUGG	International Union of Geodesy and Geophysics
IFREMER	Institut Français de Recherche pour l'Exploitation de la Mer
IOC	Intergovernmental Oceanographic Commission
ITCZ	InterTropical Convergence Zone
mEOF-r	Multivariate Empirical Orthogonal Functions reconstruction
MoM	Minutes of Meeting
NATL3D	North Atlantic 3D Ocean Currents
NEMO	Nucleus for European Modelling of the Ocean
NOAA	National Oceanic and Atmospheric Administration
NCC	Norwegian Coastal Current
NwAFC	Norwegian Atlantic Front Current
NwASC	Norwegian Atlantic Slope Current
OLCI	Ocean and Land Color Imager
OSSE	Observing System Simulation Experiment
OC	Ocean color
OSCAT	Oceansat-2 SCATterometer
PD	Product Delivery
PM	Project Manager
PMP	Project Management Plan
PUB	Publication
PUM	Product User Manual
QUID	Quality Information Document
RB	Requirement Baseline
REMSS	Remote Sensing Systems
ROMS	Regional Oceanic Modeling System
RTOFS	Real-Time Ocean Forecast System
S3	Sentinel 3
SAR	Synthetic Aperture Radar
SEVIRI	Spinning Enhanced Visible and InfraRed Imager
SCOR	Scientific Committee on Oceanic Research
SIED	Single Image Edge Detection

SKIM	Sea surface KInematics Multiscale monitoring
SLSTR	Sea & Land Surface Temperature Radiometer
SOCIB	Sistema d'observació i predicció costaner de les Illes Balears
SODA	Simple Ocean Data Assimilation Ocean/sea ice reanalysis
SSH	Sea Surface Height
SSS	Sea Surface Salinity
SST	Sea Surface Temperature
SoW	Statement of Work
TN	Technical Note
TOPAZ	Tracers of Phytoplankton with Allometric Zooplankton
TUOC	Total Upper Ocean Currents
UCL	Use Case Library
UCM	User Consultation Meeting
UCPC	Upper-layer ocean Circulation Processes e-Catalogue
UI	Upwelling Index
UN	United Nations
URD	User Requirement Document
VR	Validation Report
VT	Visualization Tool
WBS	Work Breakdown Structure
WOC	World Ocean Circulation

2 Wind-based upwelling flows and transport

2.1 Overview

Upwellings are ubiquitous, wind-driven phenomena (mostly), and they occur at various scales.

They differ in involved processes at offshore and coastal locations. Offshore, the main process which triggers an upwelling is the Ekman pumping expressed as the vertical velocity at the base of the Ekman layer. It is the consequence of the divergence of the surface Ekman transport under wind stress curl forcing. Stronger the curl, stronger the divergence of the transport and the associated upwelling. These phenomena are ubiquitous and occur at the meso-scale 0(100km). At smaller scale, SST-induced (cross-front wind gradient induced via air-sea coupling) upwelling are also ubiquitous ([RD-3]), and eddy-driven upwelling are also of concern for ocean acidification studies.

Near the shore, in addition to wind stress curl driven upwelling, another main process leading to an upwelling is driven by the coastal divergence of the Ekman transport forced by the along-shore component of the equator-ward wind flow ([RD-4], [RD-5]). The associated offshore Ekman transport causes the coastal upwelling. The various upwelling processes at work in EBUs are illustrated in Figure 1 in the case of the Benguela upwelling. Their relative importance are determined by local conditions. ([RD-6], [RD-7], [RD-8], [RD-9], [RD-10]). Indeed, large wind stress curl patterns, and the associated strong Ekman pumping vertical velocities, occur at various scales due to either a cross-shore wind gradient caused by a weakening of the wind stress very near to the shore (as shown in Figure 1) , by the presence of capes or coastal promontories and orography, or air/sea interactions in the presence of SST fronts. Pickett and Paduan (2003),([RD-8]), showed that Ekman pumping driven by the wind stress curl is at least as important as the cross-shore Ekman transport driven by the coastal divergence in the California current. Further, this cross-shore Ekman transport is generally balanced and limited by an onshore geostrophic transport (Marchesiello and Estrade, 2010, [RD-11]).

While a simple upwelling indice can be defined for open ocean conditions as a signed vertical velocity derived from the wind stress curl and associated Ekman pumping, a comprehensive upwelling indice for coastal areas should take into account the different processes and associated scales. Indeed, each process has a characteristic length that can further be regionally dependent, especially on the shape of the continental shelves and the coastal topography (Estrade et al., 2008, [RD-12]). The width of the active coastal Ekman divergence is O(10 km) (Marchesiello and Estrade, 2010, [RD-11]), depending on the slope of the shelf, while the Ekman pumping related to the wind stress curl can spread out over a much larger distance offshore (more than 100 km), which suggests disconnection of both dynamical processes in the control of coastal SST variability ([RD-11]).

Earth Observation (EO) based upwelling indices are therefore difficult to define accounting for the various upwelling processes and scales, and the situation is complicated by the fact that the ground sampling of satellite wind sensors is a compromise between coverage and resolution. For the WOC project, space monitoring of wind-driven upwelling events over the Canary upwelling region at multi-annual time scales can be performed only with past and present low resolution scatterometer and radiometer missions. Their resolution is typically a few tens of km, leaving a blind zone near the coast because of measurements contamination by land echoes. The recent wind vector climatologies that rely only on EO data (e.g. Bentamy and Croize-Fillon, 2012, [RD-14]) are sampled on a regular grid at 0.25 degree resolution in latitude and longitude, leaving the same blind zone of a few tens of km from the coast for the wind stress and wind stress curl, a zonal strip where the wind-driven upwelling processes are of paramount importance. The true resolution of these climatologies is related to their ability to sample the true scales of the wind stress variability and is not better than a few tens of km near-shore, unless a smaller scale variability is prescribed as done in Desbiolles et al., 2016, [RD-15]) to better account for the wind stress drop-off at coast.

To summarize, EO winds at this resolution show limitations to accurately estimate the wind stress over the coastal upwelling cell resulting from the active coastal Ekman divergence, to map the wind stress curl resulting from coastal orography, and likely underestimate the wind drop-off generally

observed at coast. However, these limitations will be accounted for in the definition of the upwelling indices and their interpretation.

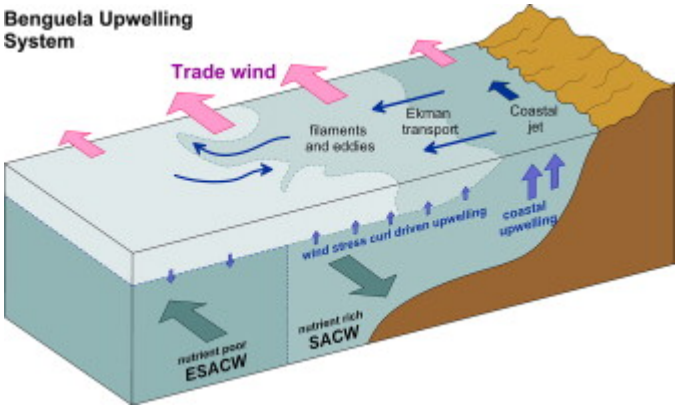

Figure 1 : Illustration of upwelling processes at work (here in the Benguela upwelling system)

short description of the products + summary of products validation

2.2 Algorithm

2.2.1 Retrieval methodology

2.2.1.1 Upwelling indices basis and implementation

Accounting for the basic concepts developed in the introduction, the two main upwelling processes shall be evaluated and quantified using EO data, i.e. the Ekman pumping and Ekman transport.

The Ekman pumping/suction is defined as the vertical velocity at the base of the Ekman layer and is related to the wind stress curl. Direct mapping and quantification of the upwelling (positive velocity) and downwelling (negative velocity) velocities is given by :

$$EKP=W_{EK}=(\mathrm{curl}\tau)/(\rho f)+(\beta\tau_x)/(\rho f^2)$$

where curlτ is the wind stress curl, ρ is the air density, f is the Coriolis parameter. The second term of the right hand part of the equation is a correction term for the β plane effect (the f derivative with latitude), and τ_x is the zonal wind stress. Details of the Ekman surface layer model and Ekman pumping calculation and interpretation can be found in several publications ([RD-16], [RD-7], [RD-17]). Units are generally given in m/s, cm/day, or m/day.

The Ekman pumping calculation does not hold very close to the coast where the surface Ekman layer merges with the bottom Ekman frictional layer.

Near the coast, the upwelling is also driven by the along-shore component of the wind stress and can be defined as the cross-shore Ekman transport by unit of coast length :

$EKT = \boldsymbol{\tau}_{\parallel}/(\rho f)$ where $\boldsymbol{\tau}_{\parallel}$ is the wind stress component parallel to the coast line. Units in m^2/s.

Both EKP and EKT are to be estimated to account for the different upwelling processes at work, but they cannot be combined easily in a single indice in terms of vertical velocity or transport. Indeed, accurate estimation of the total transport resulting from both processes would require sampling of the near-shore at less than about 10 km ([RD-18], [RD-19], [RD-15]), which is not possible with the actual EO climatologies. Alternately, it has been done using high resolution numerical regional models, as in Jacox (2018), ([RD-20]) or Pickett and Paduan (2003), ([RD-8]), but it introduces other uncertainties linked to the numerical model itself and is hardly feasible for the present study due to limited availability of high-resolution hindcasts over the time period of interest. In the frame of the present study, which aims at best exploiting the potential of the EO wind measurements, the chosen approach to combine the Ekman transport and pumping is presented in Section 4.

2.2.1.2 Input data for deriving the upwelling indices and flows

The data described hereafter are those used to estimate the EKP and EKT fields (Figure 3).
The reference wind fields are taken from the IFREMER/CERSAT and Copernicus data bases. Two different products are being used as reference : 1) the global daily and monthly fields at 0.25° resolution in latitude and longitude that are processed by using solely scatterometer data from the ASCAT/METOP missions, covering the 2007 / present time period and available at IFREMER/CERSAT ; 2) the global 6-hr, monthly fields at 0.25° resolution in latitude and longitude that are processed by using various scatterometer and radiometer data from multiple satellite missions, covering the 1992 / present time period and available at IFREMER and distributed within the CMEMS project. These two products (Bentamy et Croize-Fillion, 2012, [RD-14]) are computed using the same objective analysis (kriging algorithm) of satellite measurements, and make use of an atmospheric numerical model (ECMWF analyses and re-analyses) as background. This blended approach benefits from the global coherency of the ECMWF numerical winds patterns but is mainly weighted towards the satellite wind measurements.

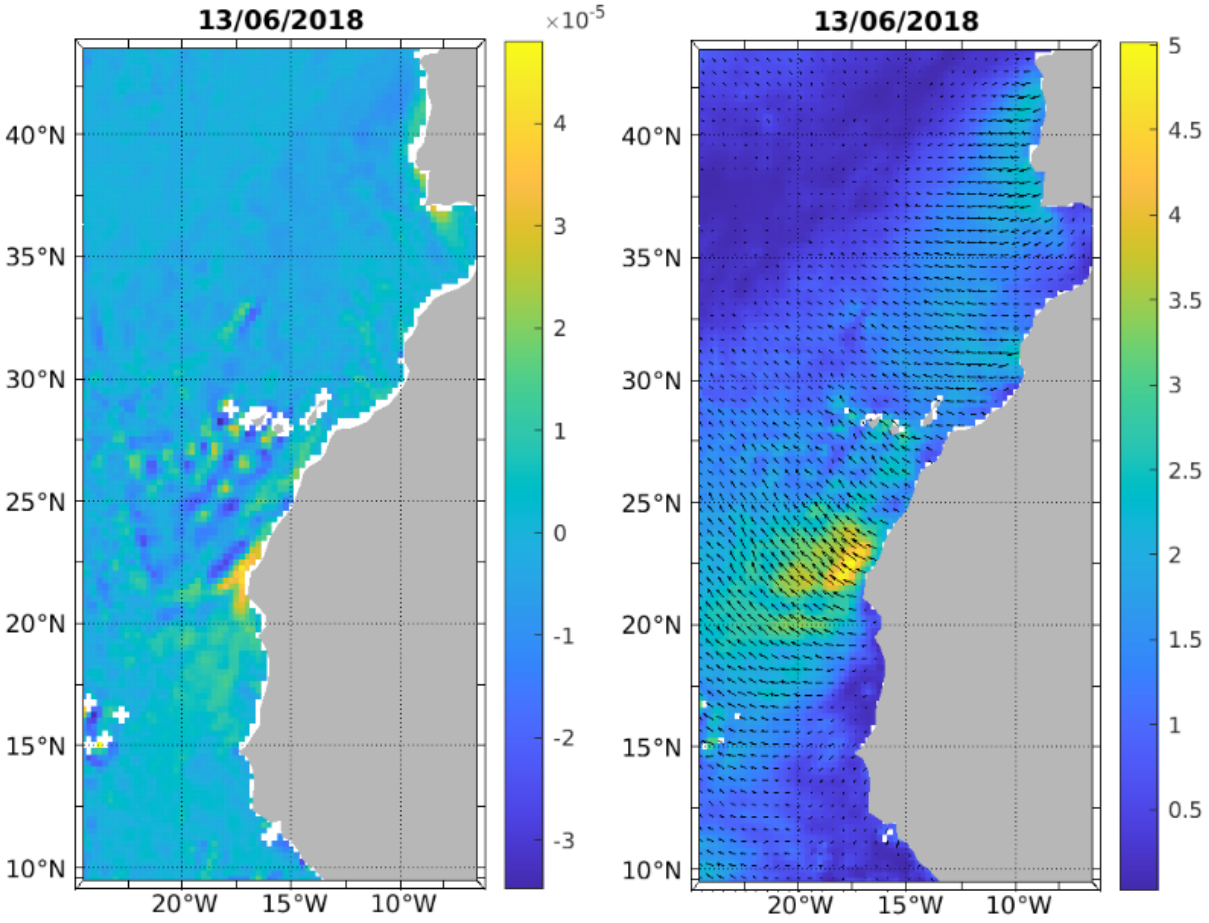

Figure 3 : Example of EKP (in $m.s^{-1}$) and EKT (in $m^2.s^{-1}$) fields computed from Ifremer winds at a 0.25° resolution (here, arrows are plotted every 2 pixels).

2.2.2 Limitations

Although the wind datasets presented in the previous section have been extensively distributed and subject to favorable validation / comparison studies (Wang et al., 2019 ; Desbiolles et al., 2016; Carvalho et al., 2014, [RD-21, RD-22, RD-15]), they however have limitations. The purpose of the present study is not the validation of wind climatologies, but it is however useful to perform a comprehensive validation by using other wind data sets in the study. Two other wind data set are being used in the same way than the IFREMER data (for calculation of upwelling indices) : The Cross-Calibrated Multi-Platform (CCMP) analysis (Atlas et al., 2011, [RD-23]) produced and distributed at Remote Sensing System (California) and the ERA5 atmospheric reanalysis produced at ECMWF (Hersbach and Dee, 2016, [RD-24]) which stands as the state of art of the most recent atmospheric re-analyses.

To give more support to the choices made for this study and to highlight limitations inherent to the different wind products, the Table 1 and Figure 2 show the results obtained by Wang et al., 2019 ([RD-21]) for the comparison between three NDBC coastal buoys (46028, 46011, 46054) located near-shore in the California upwelling system. Buoys 46028 and 46011 are located north of Point Conception, and buoy 46054 is located just to the south of Point Conception, at the western edge of Santa Barbara Channel. It shows that scatterometers (QuikSCAT or ASCAT distributed by Eumetsat) swath data at 12.5 km resolution are of very good quality, getting the best comparison results. Other data sources show lower correlations and a significant negative bias, which is due to the relatively low resolution of the regular wind grids on which the data are mapped, but also to the objective analysis used to map the data. As shown, the CCMP winds that are obtained from EO data through a 2D variational analysis show a large bias, which is still larger for atmospheric analyses or re-analyses from the WRF and MERRA numerical models. The Ifremer wind climatologies, not tested in the Wang et al. (2019), ([RD-21]) study, are derived on a 0.25 degree grid using an objective analysis that does not smooth as much the wind patterns, as shown in Quilfen, 2021 (RD-25]). Indeed, the IFREMER daily winds exhibit a larger variability than the CCMP ones, although both are derived from EO data on the same resolution grid. As discussed in [RD-25], as a result of the cross-shore wind gradient that is more or less well mapped by the different wind climatologies, the first indice (Bakun like indice) based on EKT offshore and the second one based on the sum of EKT coast and EKP integrated are very well correlated for the IFREMER and CCMP wind inputs. Although both wind products are at different resolutions and show different distribution of the wind stress curl, they however provide coherent indices whose differences are essentially related to differences in the amplitude of the wind variability (CCMP smoother than IFREMER). It therefore gives confidence in both indices and is coherent with the background physics. Conversely, this is not the case when ERA5 is used as input. Indeed, the two indices are significantly different, which may be due to the inappropriate resolution of the ERA5 fields for the upwelling studies (31 km resolution grid, but much coarser true resolution).

Table 1 Comparison statistics between buoys and various wind data sources (from Wang et al., 2019 ([RD-21]))

Table 2
Statistical metrics from the linear regression between buoy data and each of the comparison datasets.

Buoy	Dataset	Slope	Intercept	R^2	Distance from buoy (km)	Number of valid pairs
46028	QuikSCAT	0.90	1.01	0.92	5.59	5654
	ASCAT	0.94	0.25	0.94	4.91	2153
	CCMP V2	0.68	1.37	0.77	9.80	13013
	NARR	0.76	1.59	0.75	9.07	26018
	MERRA	0.59	1.69	0.74	26.85	78014
	WRF	0.38	4.88	0.15	3.64	78012
	WIND	0.79	1.13	0.83	0.62	55957
46011	QuikSCAT	0.85	1.56	0.84	4.45	5449
	ASCAT	0.89	1.02	0.84	3.55	2241
	CCMP V2	0.75	2.00	0.67	13.22	12368
	NARR	0.72	1.40	0.69	7.62	24695
	MERRA	0.62	2.04	0.64	29.07	74049
	WRF	0.39	4.77	0.14	3.24	74046
	WIND	0.77	1.65	0.73	0.89	51953
46054	QuikSCAT	0.68	2.23	0.82	4.93	3875
	ASCAT	0.81	1.16	0.88	3.77	1670
	CCMP V2	0.53	1.66	0.62	15.41	7928
	NARR	0.49	1.13	0.53	7.62	15754
	MERRA	0.40	1.76	0.58	31.41	47392
	WRF	0.37	4.91	0.16	2.10	47385
	WIND	0.80	1.45	0.79	0.99	34001

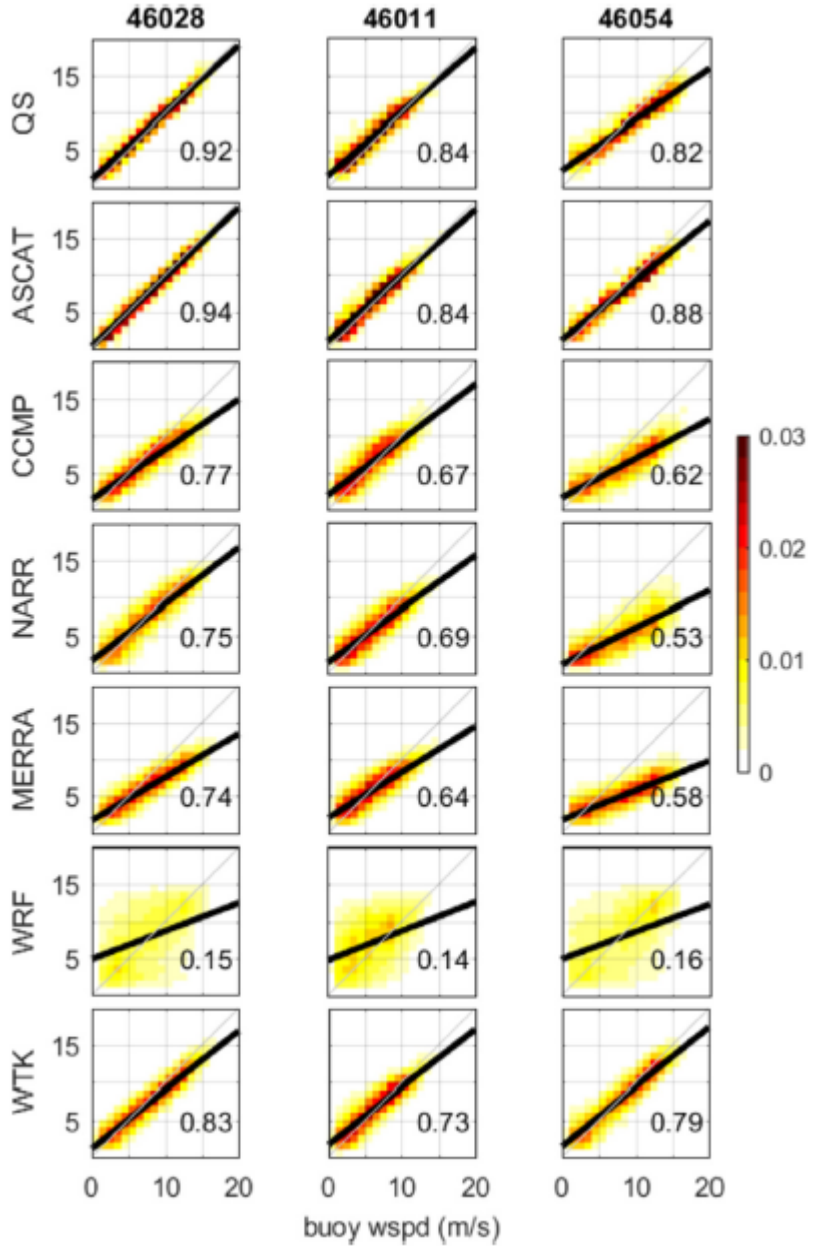

Figure 2 : Comparison between buoys and various wind data sources (from Wang et al., 2019 ([RD-21]))

2.3 Product Description

The product provide the wind-based upwelling indices and flows, i.e. EKT and EKT fields.

2.2.1 spatial information

EKP and EKT fields are provided at 0.25° resolution in latitude and longitude over the geographical region shown Figure 3.

2.2.1 temporal information

EKP and EKT fields are provided on a daily basis.

2.2.1 product content

The product contains the following variables:

wind_stress_curl
eastward_ekman_transport
northward_ekman_transport
downward_ekman_current_velocity
eastward_wind_stress
northward_wind_stress
lat
lon
time

2.2.1 file name convention

Files nomenclature is based on the date, data source and data record version.

The scheme is: <date>-WOC-L4-CURekm-CANARY_Ifremer_025_1D-v1.0-fv1.0.nc

Where date is: integer (format YYYYMMDD) corresponding to the analysis date

Example:

20181231-WOC-L4-CURekm-CANARY_Ifremer_025_1D_Quilfen2020-v1.0-fv1.0.nc

2.2.1 file format

The products are stored using the NetCDF format.

NetCDF (network Common Data Form) is an interface for array-oriented data access and a library that provides an implementation of the interface. The NetCDF library also defines a machine-independent format for representing scientific data. Together, the interface, library, and format support the creation, access, and sharing of scientific data. The NetCDF software was developed at the Unidata Program Center in Boulder, Colorado. The NetCDF libraries define a machine-independent format for representing scientific data.

Please see Unidata NetCDF pages for more information, and to retrieve NetCDF software package.

NetCDF data is:

* Self-Describing. A netCDF file includes information about the data it contains.

* Architecture-independent. A NetCDF file is represented in a form that can be accessed by computers with different ways of storing integers, characters, and floating-point numbers.

* Direct-access. A small subset of a large dataset may be accessed efficiently, without first reading through all the preceding data.

* Appendable. Data can be appended to a NetCDF dataset along one dimension without copying the dataset or redefining its structure. The structure of a NetCDF dataset can be changed, though this sometimes causes the dataset to be copied.

* Sharable. One writer and multiple readers may simultaneously access the same NetCDF file.

NetCDF data can be browsed and used through a number of software, like:

- ncBrowse: http://www.epic.noaa.gov/java/ncBrowse/,
- NetCDF Operator (NCO): http://nco.sourceforge.net/
- IDL, Matlab, GMT…

Useful information on UNIDATA: http://www.unidata.ucar.edu/software/netcdf/

Example:

```
netcdf \20181226-WOC-L4-CURekm-CANARY_Ifremer_025_1D_Quilfen2020-v1.0-fv1.0 {
dimensions:
    lat = 140 ;
    lon = 76 ;
    time = 1 ;
variables:
    double wind_stress_curl(lat, lon) ;
        wind_stress_curl:_FillValue = 1.e+20 ;
        wind_stress_curl:long_name = "wind stress curl" ;
        wind_stress_curl:units = "s-1" ;
    double eastward_ekman_transport(lat, lon) ;
        eastward_ekman_transport:_FillValue = 1.e+20 ;
        eastward_ekman_transport:long_name = "zonal component of Ekman transport" ;
        eastward_ekman_transport:units = "m2 s-1" ;
    double northward_ekman_transport(lat, lon) ;
```

northward_ekman_transport:_FillValue = 1.e+20 ;

northward_ekman_transport:long_name = "meridional component of Ekman transport" ;

northward_ekman_transport:units = "m2 s-1" ;

double downward_ekman_current_velocity(lat, lon) ;

downward_ekman_current_velocity:_FillValue = 1.e+20 ;

downward_ekman_current_velocity:long_name = "Ekman vertical velocity (<0 = Ekman pumping; >0 = Ekman suction)" ;

downward_ekman_current_velocity:units = "m s-1" ;

downward_ekman_current_velocity:positive = "down" ;

double eastward_wind_stress(lat, lon) ;

eastward_wind_stress:_FillValue = 1.e+20 ;

eastward_wind_stress:standard_name = "surface_downward_eastward_stress" ;

eastward_wind_stress:long_name = "zonal component of 10m wind stress" ;

eastward_wind_stress:units = "Pa" ;

double northward_wind_stress(lat, lon) ;

northward_wind_stress:_FillValue = 1.e+20 ;

northward_wind_stress:standard_name = "surface_downward_northward_stress" ;

northward_wind_stress:long_name = "meridional component of 10m wind stress" ;

northward_wind_stress:units = "Pa" ;

float lat(lat) ;

lat:_FillValue = 1.e+20f ;

lat:least_significant_digit = 3LL ;

lat:axis = "Y" ;

lat:standard_name = "latitude" ;

lat:units = "degree_north" ;

lat:valid_range = -90.f, 90.f ;

float lon(lon) ;

lon:_FillValue = 1.e+20f ;

lon:least_significant_digit = 3LL ;

lon:axis = "X" ;

lon:standard_name = "longitude" ;

lon:units = "degree_east" ;

lon:valid_range = -180.f, 180.f ;

int time(time) ;

time:_FillValue = 0 ;

time:axis = "T" ;

time:standard_name = "time" ;

time:long_name = "measurement time" ;

time:units = "seconds since 1981-01-01T00:00:00+00:00" ;

time:calendar = "proleptic_gregorian" ;

// global attributes:

:Conventions = "CF-1.7, ACDD-1.3, ISO 8601" ;

:Metadata_Conventions = "Climate and Forecast (CF) 1.7, Attribute Convention for Data Discovery (ACDD) 1.3" ;

:standard_name_vocabulary = "NetCDF Climate and Forecast (CF) Metadata Convention version 1.8" ;

:title = "Ekman transport and pumping from Ifremer wind over the Canary Upwelling System, for ESA WOC project" ;

:summary = "This dataset contains daily estimation of the Ekman transport vector and vertical pumping over the Canary Upwelling System computed from Ifremer winds" ;

:id = "WOC-L4-CURekm-CANARY_Ifremer_025_1D_Quilfen2020" ;

:institution = "Institut Francais de Recherche pour l\'Exploitation de la mer / LOPS, Institut Francais de Recherche pour l\'Exploitation de la mer / CERSAT, European Space Agency" ;

:institution_abbreviation = "Ifremer/LOPS, Ifremer/Cersat, ESA" ;

:references = "Y. Quilfen, J. Shutler, J.-F. Piolle, E. Autret, Recent trends in the wind-driven California current upwelling system, Remote Sensing of Environment, Volume 261, 2021, 112486, ISSN 0034-4257, https://doi.org/10.1016/j.rse.2021.112486. (https://www.sciencedirect.com/science/article/pii/S0034425721002042)" ;

:product_version = "1.0" ;

:keywords = "Earth Science > Oceans > Ocean Circulation > Ocean Currents, Earth Science > Oceans > Ocean Circulation > Upwelling/Downwelling" ;

:keywords_vocabulary = "NASA Global Change Master Directory (GCMD) Science Keywords" ;

:naming_authority = "fr.ifremer.cersat" ;

:cdm_data_type = "grid" ;

:comment = "These data were produced at Ifremer as part of the ESA WOC project." ;

:creator_name = "Yves Quilfen" ;

:creator_url = "https://www.umr-lops.fr" ;

:creator_email = "yves.quilfen@ifremer.fr" ;

:creator_institution = "Ifremer / LOPS" ;

:project = "World Ocean Circulation (WOC) - European Space Agency" ;

:time_coverage_start = "2018-12-26T00:00:00Z" ;

:time_coverage_end = "2018-12-27T00:00:00Z" ;

:geospatial_lat_min = 9. ;

:geospatial_lat_max = 44. ;

:geospatial_lat_units = "degree_north" ;

:geospatial_lon_min = -25. ;

:geospatial_lon_max = -6. ;

:geospatial_lon_units = "degree_east" ;

:geospatial_vertical_units = "meters above mean sea level" ;

:geospatial_vertical_positive = "up" ;

:spatial_resolution = "0.25 degree" ;

:license = "ESA WOC Data Policy: free and open access" ;

:acknowledgement = "Please acknowledge the use of these data with the following statement: these data were obtained from the ESA WOC project" ;

:format_version = "WOC v1.0" ;

:processing_level = "L4" ;

:method = "https://doi.org/10.1016/j.rse.2021.112486" ;

:track_id = "c95050d2-4014-4c0d-afc8-bfd7941a810b" ;

:publisher_name = "CERSAT" ;

:publisher_url = "cersat.ifremer.fr" ;

:publisher_email = "cersat@ifremer.fr" ;

:publisher_institution = "Ifremer / CERSAT" ;

:scientific_support_contact = "yves.quilfen@ifremer.fr" ;

:technical_support_contact = "cersat@ifremer.fr" ;

:key_variables = "eastward_ekman_transport, northward_ekman_transport, downward_ekman_current_velocity" ;

:date_created = "2021-06-29T19:42:34.062339" ;

:date_modified = "2021-06-29T19:42:34.062352" ;

:source = "Quilfen/Matlab" ;

:source_version = "1.0" ;

:history = "2021_05-28 11:34:00 - Creation" ;

:input = "20181226_CAN.mat" ;

:processing_software = "Quilfen/Matlab 1.0" ;

}

3 SST-based upwelling indices

3.1 Overview

This chapter presents SST-based upwelling indices. The method and the data used in the generation of the SST-based upwelling indices are presented in section 3.2.

3.2 Algorithm

3.2.1 Retrieval methodology

2.2.1.1 Input data for SST-based indices

Index calculations are based on SST data from the European Space Agency Sea Surface Temperature Climate Change Initiative (ESA SST CCI) analysis product (1982-2016) and from the Copernicus Climate Change Service (C3S) product (2016-2018). The CCI dataset provides a climate data record of global SST data derived from satellite thermal infra-red measurements from 11 Advanced Very High Resolution Radiometers (AVHRRs) and three Along-Track Scanning Radiometers (ATSRs). The C3S dataset contains data from AVHRRs and from the Sea and Land Surface Temperature Radiometer (SLSTR) on-board SENTINEL-3. The L4 product uses these observations to provide daily global gap-free SST fields at a 0.05° horizontal grid resolution. In-situ data are not used in the L4 reconstruction. The gridded SST product is intended to represent a daily-mean SST field at 20 cm depth. The method used to reconstruct gap-free fields is variational assimilation. The lack of input data is mainly due to cloudy conditions but in upwelling regions, possible «over masking» can occur, especially over the cold coastal waters or over intense SST fronts. An example of the L4 daily product is shown Figure 4 for the Canary upwelling region. The spatial and temporal resolution of the L4 fields is very high (0.05° and daily respectively) but the effective spatial resolution is coarser (Reynolds et al., 2013, [RD-26]), the smoothing inevitably occurring when in-filling sparse observations. However particular attention has been paid in the parametrization of the error covariance to preserve SST features (Merchant et al., 2019, [RD-27]). Very detailed presentation of the dataset and global validation results are given in [RD-27].

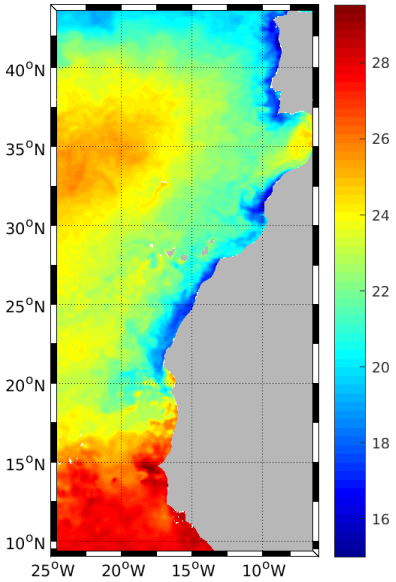

Figure 4 : example of daily SST from ESA CCI SST dataset over the Canary upwelling region

2.2.1.1 Upwelling characterization from SST data

SST-based upwelling indices have been taken as a thermal difference between the coastal and the offshore SST taken at the same latitude, in order to quantify the coastal cooling effect of the upwelling (Wooster et al., 1976; Nykjær and Van Camp, 1994 : [RD-28], [RD-29]) :

$$UI_{\Delta SST} = SST_{offshore} - SST_{upw}$$

The index is defined at each latitudinal point. Many ways to define SST_{upw} and $SST_{offshore}$ have been proposed in the litterature (see more details in the section dedicated to the validation hereafter). The first method used here is based on the Gaussian Mixture Model (GMM). This method is a probabilistic model assuming that all the data points are generated from a mixture of a finite number of Gaussian distributions (with unknown parameters and a covariance of the difference classes that can be constrained). GMM has been proposed to compute upwelling indices in the frame of the ESA OceanSODA project. In addition to UI estimates, the method allows to determine « the upwelling area », giving the variable $U_{extension}$ in km for each latitudinal point. It can be applied on monthly or daily data. An example of application is shown in Figure 5. Given the inhomogeneity of the whole area in terms of seasonal variability of the system, the method is applied for several predefined sub-regions (table 2). The main characteristics of those regions are the following : the Iberian region is characterized by a high seasonality, the "Morocco region" by a low seasonality and lower UIs, the "Western Sahara" area by a very low seasonality and high indices and the "Senegal-Mauritania" region by a very high seasonality.

The number of clusters has been fixed to 3 for three following sub-areas : Senegal, Western Sahara, Morocco and to 4 for the Iberian region, given results of the combination of two criteria

(Davies-Bouldin et Silhouette Coefficient) applied for all regions and over the time period 2001-2015.

The "upwelling region" is defined as the "coldest cluster" (if this region is the closest to the coast, otherwise, it is considered there is no upwelling and the values of the indices are not defined).

In addition to the indices defined by the GMM, two basic indices based on the following definitions are provided : the first one with $SST_{offshore}$ at 5° to the coast, the second one with $SST_{offshore}$ at 3.5° to the coast, both with and SST_{upw} in the coastal band (SST minimum in the 3-pixel band closest to the coast). All indices are given at each latitudinal point.

Table 2 : The GMM has been applied over 4 regions.

Area	latitude min	latitude max	longitude min	longitude max
Iberian	37.5°N	43.5°N	25°E	6°E
Morocco	26°N	36°N	25°E	6°E
Western Sahara	21°N	26°N	25°E	12°E
Senegal Mauritania	9°N	21°N	25°E	12°E

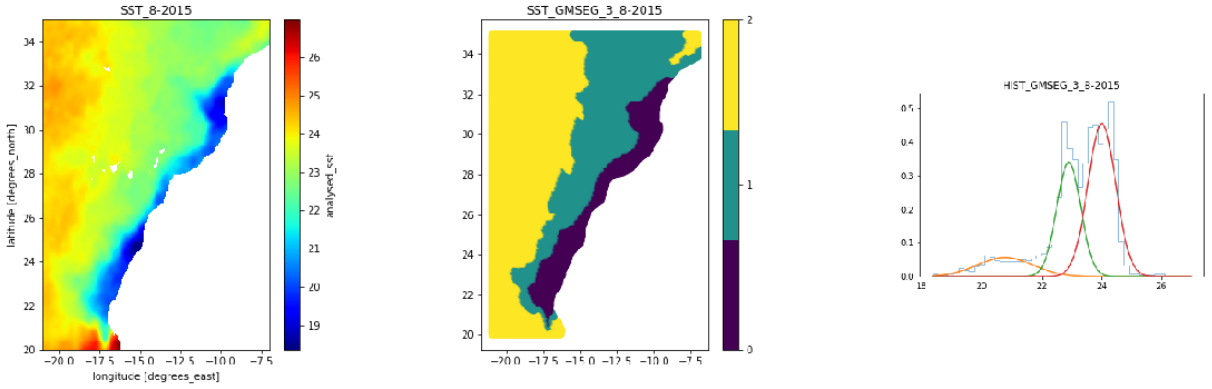

Figure 5 : Example of monthly mean of SST in the Canary upwelling system (left), segmentation with 3 regions (middle) and the associated distributions (right).

2.2.2 Limitations

Input data

Input SST fields have been validated against drifters and moorings (dedicated CCI dataset). The number of match-ups is highly variable in space and time as shown in 6a. The validation is mainly done from the end of the 90's as shown by the time series of number of match-ups for each month for the Canary region presented in Figure 6c. Figure 6a presenting the number of match-ups (on a 0.25°x 0.25° grid) for the Canary upwelling region show a very heterogeneous spatial distribution with very few observations in the Tropical area and along the African coasts. The validation results over the show a very good agreement with in-situ observations (drifting buoys) with a mean bias of -0,08 °C and a standard deviation of 0,04 °C, even though a large scale bias is observed in the Tropical Atlantic (but from a limited match-up dataset). The conclusion is that there is no significant bias over the coastal surface waters whereas warm biases would be expected in case of strong smoothing or "over masking".

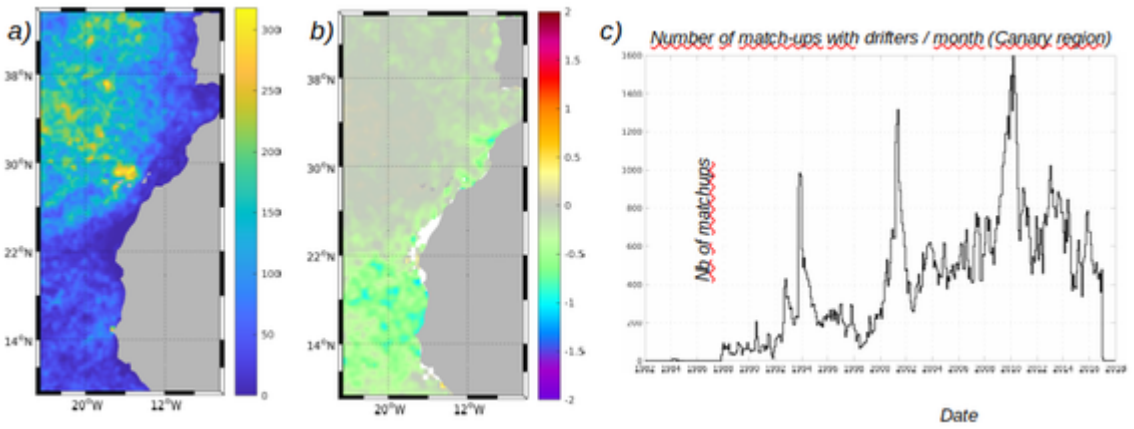

Figure 6 : Comparison of the input SST data set against drifting buoys. a) Number of match-ups (mean on a 0.25°x0.25° grid). b) Mean biases (on a 0.25°x0.25° grid) in degree Celsius. c) Monthly mean of number of match-ups in the Canary region.

Method and results

The way both thermal references are chosen in the literature is always arbitrary. Previous SST-based indices make use of various locations of SST max at arbitrary distances from the coast, whereas the coastal reference itself is measured over various widths. The offshore position was chosen at 500 km from the coast whereas the most coastal SST was systematically used as the SST min reference (Nykjær and VanCamp (1994), Marcello et al. (2011), [RD-29, RD-30]). Santos et al., 2005 ([RD-31]) found that the general patterns of the spatio-temporal variability of their SST-based index were similar within the range 400–1000 km offshore. Lathurilère et al. 2008 ([RD-32]) chose the

SST average in the band located within 500–700 km from the coast. Segmentation methods have also been used. Here, several methods have been tested and compared yielding to choose the GMM segmentation method to estimate the contour of the upwelling area and thus allowing the estimation of the local upwelling extension, in addition to UI:

- K-means (e.g. Nascimento et al., 2009 [RD-33])
- Gaussian Mixture Models : probabilistic model
- Fuzzy C-means clustering (e. g. Nascimento and Franco, 2009([RD-34]), Nascimento et al. 2009 ([RD-33]), Souza et al., 2008 ([RD-35]))
- Otsu algorithm : automatic thresholding method such as the between-class variance is maximized (e. g. Tamim et al., 2015 ([RD-36]), Nascimento et al., 2015([RD-37])

It is difficult to compare the different methods and results since the references are defined by different criteria and the input data sets and the considered time period are different. The 4 segmentation methods have been tested on a one-year data set (2015). The evaluation of the methods have been done visually.

In this work we have taken the opportunity to produce indices from the new ESA CCI SST and C3S data sets providing a long and homogeneous time series input data set and allowing future updates of the SST-based indices thanks to the regular updates of the C3S data.

As mentioned in the previous section, the number of clusters has been fixed given results of the combination of two criteria (Davies-Bouldin et Silhouette Coefficient) applied for all sub-regions and in the time period 2001-2015.

3.3 Product Description

The product provides the SST-based upwelling indices at each latitudinal point.

3.2.1 spatial information

SST_based indices are provided at 0.05° resolution in latitude

3.2.1 temporal information

SST_based indices are provided on a daily and a monthly basis. The clustering method is applied only on monthly data.

3.2.1 product content

The product provides three different upwelling indices. The user can start his work with the variable called ui1_sst, i.e. the upwelling index (at each latitudinal point) defined with SST_{upw} the minimum SST value in a coastal band and $SST_{offshore}$ the SST value at 3.5° off the coast. The product contains the following variables:

variable name	**description**
latitude	latitude (in degrees North)
time	seconds since 01/01/1981
ui1_sst	upwelling index (at each latitudinal point), in degrees Celsius, defined as : SST_{upw} is the minimum SST value in a coastal band (between the shoreline and 3 pixels of 0.05° in longitude off the coast). $SST_{offshore}$ is the SST value at 3.5° off the coast.
ui1_min_sst_upw	SST_{upw}, in degrees Celsius, is the minimum SST value in a coastal band (between the shoreline and 3 pixels of 0.05° in longitude off the coast).
ui1_min_sst_upw_lon	longitude of SST_{upw}
ui1_max_sst_lon	longitude of $SST_{offshore}$
ui1_quality_level	quality level of the index. 0: upwelling in the coastal band 1: no upwelling
shoreline	shoreline longitude at each latitudinal point
coastal_fringe	longitude of the west coastal band boundary
	only in monthly files
ui2_sst_gmm	upwelling index, in degrees Celsius, from the clustering method (gmm for Gaussian Mixture Model) 1 : SST_{upw} is the minimum SST value in the upwelling region (at each latitudinal point) defined by the clustering method. $SST_{offshore}$ is the maximum SST value (at each latitudinal point) out of the upwelling region.
ui3_sst_gmm	upwelling index, in degrees Celsius, from the clustering method (gmm for Gaussian Mixture Model) 2 : SST_{upw} is the minimum SST value in the upwelling region (at each latitudinal point) defined by the clustering method. $SST_{offshore}$ is the maximum SST value (at each latitudinal point) at 3.5° off the coast.
ui2_min_sst_upw	minimum SST value used to calculate ui2_sst_gmm
ui3_min_sst_upw	minimum SST value used to calculate ui3_sst_gmm
ui2_min_sst_upw_lon	longitude of SST_{upw}used to calculate ui2_sst_gmm
ui3_min_sst_upw_lon	longitude of SST_{upw} used to calculate ui3_sst_gmm

ui2_quality_level	quality level of the index 0: coastal upwelling 1: upwelling not along the coast 2: no upwelling area
ui3_quality_level	quality level of the index 0: coastal upwelling 1: upwelling not along the coast 2: no upwelling area
upw_ext	upwelling extent in km

3.2.1 file name convention

Files nomenclature is based on the date, data source and data record version.

The scheme is: <date>-WOC-SSTindex-CANARY_Ifremer_005_1D-v1.0-fv1.0.nc

Where date is: integer (format YYYYMMDD) corresponding to the analysis date

Example:

20181231-WOC-L4-CURekm-CANARY_Ifremer_025_1D_Quilfen2020-v1.0-fv1.0.nc

3.2.1 file format

The products are stored using the NetCDF format.

4 Wind-based and SST-based upwelling indices at stations

4.1 Overview

This chapter presents the product providing upwelling indices at predefined stations.

4.2 Algorithm

4.2.1 Retrieval methodology

In the frame of the present study, which aims at best exploiting the potential of the EO wind measurements, the chosen approach is based on the definition of two different wind-driven

upwelling indices: 1) the classical Bakun, 1973 ([RD-4]) like indice, based solely on an offshore estimation of EKT; 2) an indice combining the Ekman transport and pumping in a more realistic way following the background discussed in section 1, computed as the sum of EKP (integrated from an offshore location to the coast) and EKT at the location (as sampled by the EO climatology) the closest to the coast as in Halpern, 2002 ([RD-7]), or Pickett and Paduan, 2003 ([RD-8]). It has been often argued that the Bakun indice, calculated at offshore locations, generally mitigates for the use of low resolution data because it favorably balances, in case of cross-shore wind gradient, between its overestimation of the cross-shore Ekman transport due to the coastal divergence and the lack of the Ekman pumping contribution in its definition. However, although the Bakun index has been widely used for decades or many applications such as for fisheries monitoring and can be better estimated with recent EO, it can certainly be favorably associated for assessment with the proposed second indice estimated as the sum of the integrated EKP and EKT estimated at coast.

Therefore, to monitor and characterize the upwelling transports and velocities over the entire regions of interest, a series of monitoring stations are defined as displayed in Figures 7 for the Canary upwelling system. The stations are located every two degrees in latitude, to cover the full upwelling system, and at longitudes that satisfy the following two conditions: to be representative of near-shore conditions, i.e. locations ~ 100 km from the coast which is the strip where climatic modulations of the acidification trends are the larger (Turi et al., 2016 ([RD-38]), and to be located between the mean summertime limit of zero EKP and the mean summertime EKP maximum (for correct integration of EKP from the station to the coast). Stations latitudes and longitudes, distances to coast, coast angles (for EKT calculation and EKP integration), depth, and longitudes and latitudes of the coastal point the nearest to the stations are given in Table 3. As shown, all stations satisfy the above conditions, are by more than 300 m depth and at a distance of about 100 km from the coast.

For calculation of the alongshore wind stress (to compute EKT) and integration of EKP along the distance from station to coast, the coast orientation has been determined and transects defined for each station as shown in Figure 8. For illustration, the Figure 8 presents also the mean summertime sea surface temperature (SST) in 2010 derived from the OSTIA analyses.

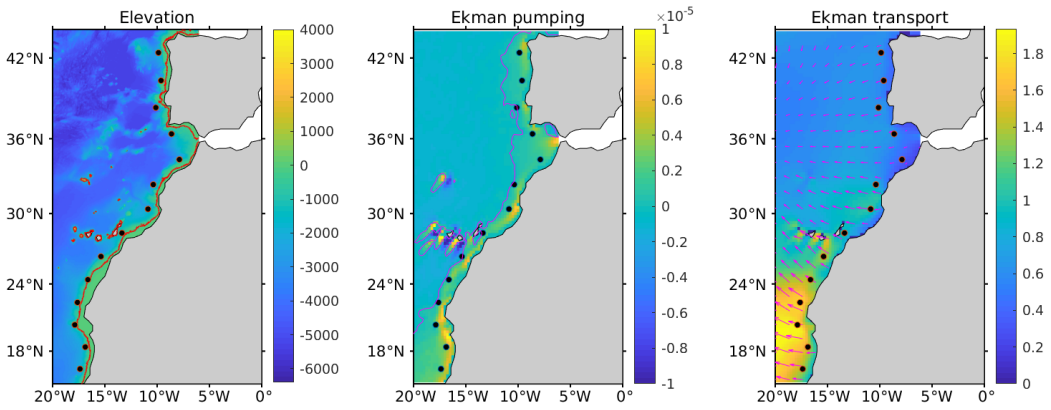

Figure 7 : The Canary upwelling region with observation stations as black dots. (left) : seafloor elevation (m) and -100 m contour (red solid line) ; (middle) : mean summer (JJA) Ekman pumping ($m.s^{-1}$) and isocontour zero (magenta solid line) ; (right) : mean summer (JJA) Ekman transport magnitude ($m^2.s^{-1}$) and direction (arrows).

Table 3: Offshore location of the Canary upwelling observation stations shown in Figure 7 (two first columns), distance to coast (km), seafloor elevation (m), coast angle (degrees relative to the zonal axis pointing east) at the closest coast location (two last columns).

Station	Longitude	Latitude	D2coast	Depth	Coast angle	Longitude_coast	Latitude_coast
1	-17.375	16.375	102.0	2092	78.0	-16.469	16.086
2	-16.875	18.375	87.5	1283	103.4	-16.105	18.666
3	-17.875	20.375	108.5	864	129.3	-16.720	20.860
4	-17.625	22.375	99.5	1890	65.9	-16.750	21.997
5	-16.625	24.375	109.6	741	59.5	-15.723	23.833
6	-15.375	26.375	102.3	1718	68.3	-14.461	25.961
7	-13.375	28.375	85.9	1189	26.1	-12.780	27.807
8	-10.875	30.375	109.4	1918	83.7	-9.747	30.250
9	-10.375	32.375	99.9	2928	63.7	-9.397	32.027
10	-7.875	34.375	83.8	1768	28.1	-7.417	33.723
11	-8.625	36.375	84.4	2683	174.0	-8.483	37.127
12	-10.125	38.375	94.3	4695	119.0	-9.172	38.777
13	-9.625	40.375	71.6	2892	78.4	-8.807	40.223
14	-9.875	42.375	79.6	2214	102.6	-8.917	42.473

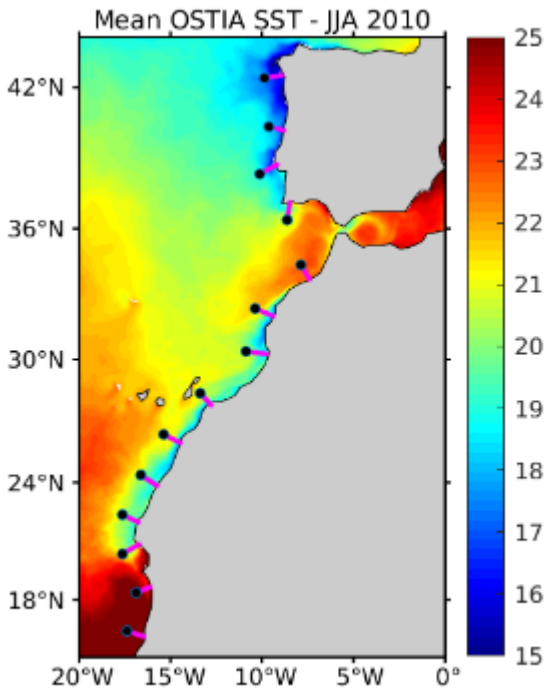

Figure 8 : Mean summertime OSTIA SST in 2010 for the Canary (right) and California (left) upwelling regions with observation stations as black dots and the perpendicular to coast along which EKP is integrated as solid magenta lines.

4.2.2 Limitations

As discussed in [RD-25], as a result of the cross-shore wind gradient that is more or less well mapped by the different wind climatologies, the first indice (Bakun like indice) based on EKT offshore and the second one based on the sum of EKT coast and EKP integrated are very well correlated for the IFREMER and CCMP wind inputs. Although both wind products are at different resolutions and show different distribution of the wind stress curl, they however provide coherent indices whose differences are essentially related to differences in the amplitude of the wind variability (CCMP smoother than IFREMER). It therefore gives confidence in both indices and is coherent with the background physics. Conversely, this is not the case when ERA5 is used as input. Indeed, the two indices are significantly different, which may be due to the inappropriate resolution of the ERA5 fields for the upwelling studies (31 km resolution grid, but much coarser true resolution).